REQ. NO. 1-9033

CONTRACT REPORT NO. 05U81-00226

Elutriation Rates from Fluidized Bed Combustors and from Cold Fluidized Beds of FBC Product Particles: Technical Report

B.-S. Xu, H.A. Becker and B.K. Code
Department of Chemical Engineering
Queen's University at Kingston
Kingston, Canada

49 pp

Technical Report QFBC.TR.83.2
Queen's Fluidized Bed Combustion Laboratory

Prepared for
Energy Mines and Resources Canada
Energy Research Laboratories, CANMET
Ottawa, Canada

ELUTRIATION RATES FROM FLUIDIZED BED COMBUSTORS AND FROM COLD FLUIDIZED BEDS OF FBC PRODUCT PARTICLES[a]

Bing-Song Xu[b], M.A. Becker and R.K Code
Dept. of Chemical Engineering
Queen's University at Kingston
Kingston, Canada K7L 3N6

Paper for presentation at the First International
Fluidized Bed Combustion and Applied Technology
Symposium in the People's Republic of China,
Aug. 22-26, 1983, Beijing

---

[a] Issued as technical report QFBC.TR.83.2,
Queen's Fluidized Bed Combustion Laboratory

[b] Visiting Scholar at Queen's University,
1982-83. Home address:
Shandong Engineering Institute, Jinan,
Shandong, The People's Republic of China

ABSTRACT

Particle elutriation rates were measured in pilot plant trials on the combustion of high-sulphur coal with limestone addition for sulphur capture. A cold-modelling system was also built with which elutriation was studied over a broad range of operating conditions using spent bed material from the pilot plant trials. Attention is particularly focussed on the division of the solids leaving flux between elutriated particles and bed product. For a given particle diameter D_p, this division appears to be determined primarily by the ratio $D_p/v^{1.163}$, where v is the fluidizing velocity, and by the recycle level. A generalized correlation of the results is suggested.

1. INTRODUCTION

1.1 The problem considered

In the continuous, steady-state operation of a fluidized-bed combustor burning coal, with the addition of limestone for sulphur capture, the system receives coal and limestone as the solid feedstreams. The solid residues from reaction leave the bed in two streams: (a) as a product stream of bed solids drained directly from the bed--the "bed product", and (b) as elutriated particles transported by the exhaust gases. The exhaust gases normally pass through dust removal equipment (cyclone separators, bag filters, electrostatic precipitators), and a part of the dust separated may be recycled. If the process were carried out very gently, then the product particle characteristics would tend to be uniquely determined by the coal and limestone as fed. In fact, however, size reduction (by abrasion and stress-induced breakage) and enlargement (by agglomeration) are usually significant, especially the former, so the output cannot entirely be predicted from the input. In any case, there is a predictable mass of solids leaving the combustor, with typically a fairly broad particle size distribution. The question asked here is, for each size of particle, how will the mass flux be split between the leaving streams? Attention is focussed not only on what is elutriated, but also on what is not elutriated. By examining both aspects at once, more progress may be possible than if only one or the other is approached in isolation.

1.2 State of the field

It is fairly generally accepted that the elutriation rate of particles of a given diameter, D_p, is proportional to the concentration of particles of that diameter in the bed:

$$\dot{m}_{D,e} = K_D A_b w_D \ , \qquad (1)$$

where

$$\int_0^\infty \dot{m}_{D,e}\, dD_p = \dot{m}_e \ ,$$

$$\int_0^\infty w_D\, dD_p = 1 \ ,$$

$\dot{m}_{D,e}\, dD_p$ is the mass flux of elutriated particles in the size range $(D_p, D_p + dD_p)$, $w_D\, dD_p$ is the mass fraction of the bed solids in that range, and K_D is the elutriation coefficient for particles of diameter D_p. Considerable effort has been given [2, 6, 7, 13, 15, 17--28] to characterizing and predicting the coefficient K_D. An interesting finding is that of Wen and Hashinger [19] who showed that K_D is effectively independent of the particle size distribution.

Osberg and Charlesworth [17] considered the difference between the freeboard gas velocity and a particle's terminal free-fall velocity to be the driving force for elutriation. Theory based on this idea has been elaborated by others, e.g.

Wen and Hashinger [19] and Yagi and Aochi [28]. A complete theory, of course, must answer not only the question of which particles will be elutriated once they get up in the freeboard, but also the more complex problem of how they leave the bed in the first place. It is commonly agreed that bubble eruption at the bed surface is the main mechanism for particle ejection. Merrick and Highley [15] used the ratio $(v - v_{mf})/v_{mf}$ as a measure of the intensity of bubble eruption, thereby attaching importance to the minimum fluidizing velocity v_{mf} as a factor affecting elutriation. Zenz and Weil [21] developed a model and a correlation, later modified by Lin, Sears and Wen [13], based on the bubble eruption mechanism. Zachovin, Beer and Sarofim [2] developed another correlation. Some investigators [7, 8, 9, 13] have compared their own experimental data with the predictions of published correlations. Geldart, et al. [7] observed that, "None of the existing correlations adequately predicts our data." Gugnoni and Zenz [9] in like vein found that, "In no instance can the agreement be deemed satisfactory." Some of the correlations in fact suggest unlikely conclusions such as increase of elutriation with increasing particle size and density and with decreasing gas viscosity. In short, no correlation yet proposed has been demonstrated to be generally sound and reasonably accurate. Significant progress has been made in understanding the phenomenology of particle elutriation from fluidized beds, but present knowledge is weak in predictive power and therefore presumably deficient in physical insight, or else the problem is of such complexity that results cannot be reduced to any simple

formula or "correlation".

1.3 Occasion for the present work

Research at Queen's University on atmospheric fluidised-bed combustion has been in progress since 1979, as part of a Canadian program of research and development on FBC coordinated and sponsored by Energy, Mines and Resources Canada, the department of the Government of Canada charged with responsibility for energy. At the heart of the effort is an AFBC pilot-plant with a maximum coal burning capacity of 100 kg/hr. Various bench-scale systems have also been built for basic studies supporting the pilot plant trials. The work is particularly concerned with some outstanding Canadian candidate fuels for FBC, such as coal from the Maritime provinces and tar-sands coke from the province of Alberta, both with sulphur contents up to 8 % and both available in great quantity, ready resources waiting for an appropriate technology.

The Queen's AFBC pilot plant has been described in a recent report [3], as have the pilot plant trials up to April, 1983 [4]. In the course of these trials, data were obtained on elutriation over a broad range of operating conditions. The work described in the present paper was conceived to utilise these data, with the help of a supporting cold-modelling study, to advance the understanding and quantitative treatment of this important phenomenon.

1.4 On the design of the experiments

The pilot plant combustion trials were not designed to study elutriation as such but nevertheless provided a reasonably broad range of relevant conditions centred, of course, around the optimum points for combustion and sulphur capture.

The cold-modelling studies were done with a rig having, like the pilot-plant, the features common to most operating FBC systems: a continuous supply of particles and a continuous discharge, with interest focussed on the steady-state. The solid feed material used was bed product from the pilot-plant operations. The rig easily permitted operation over wide ranges of bed depth and fluidizing velocity and thus complemented the pilot plant work. The results obtained with the two systems--pilot plant and cold model--moreover allow a testing of the validity of cold modelling for simulating elutriation from an FBC combustion system. The cold model was, after all, in many ways markedly different from the pilot plant and other operating FBC systems:

- the bed was of small diameter
- there were no in-bed tubes to simulate the effect of an in-bed heat-exchanger tube array
- the air distributor plate was simply a porous plate rather than an array of bubble caps or jet injection heads.

2. EXPERIMENTAL

2.1 The pilot plant

The general features of the pilot plant that are of present interest are shown in Fig. 1. Recycle of dust separated in the cyclone was provided for, at levels ranging from total recycle to none. There were in total three solids product streams: the bed product (solids drawn directly from the bed), the cyclone product (the cycloned dust not recycled), and the baghouse product.

The combustion chamber was nearly square in plan, 381 mm by 406 mm, of 0.155 m^2 area. The chamber height, from distributor plate to top of open freeboard, was 3.3 m. The distributor plate incorporated a uniform array of 100 distributor heads, each providing four horizontal jets. Bed height (or depth) in the trials of present interest was controlled by gravity overflow from a port 1.19 m above the distributor plate. A more common method is to mechanically extract bed solids from the side or bottom of the bed. The combustor has provision for such extraction from a port in the side, near the bottom, and this will be used in some future trials.

Between 12 and 24 heat exchanger tubes were provided for in-bed heat exchange. The presence of these certainly affected the bed dynamics and thus the quality of fluidization.

A detailed description of the system may be found in the reports [3, 4] mentioned earlier.

2.2 The cold-modelling rig

The basic features of the cold modelling rig are indicated in Fig. 2. Solids were fed from a pressurized feeder-hopper in which the overhead air space was pneumatically connected to the air plenum chamber at the bottom of the fluidized-bed "column", beneath the distributor plate. A helical feeder with variable-speed drive provided a very uniform feedrate. The freeboard gases were collected by a movable conical hood or "probe" and then passed through a cyclone separator to remove the dust (the amount escaping in the leaving gas stream was negligible).

The column was of transparent plastic pipe, 150 mm I.D. It was made of sections coupled together, and could be made up to 6 m high. As in the pilot plant, the solids feed mode was "underbed", through a port near the bottom of the bed. Again, bed height was controlled by gravity overflow. The bed height was varied by changing the position of the column section containing the overflow port. There was no provision for recycle of cycloned dust; this will, though, be considered for any future work.

2.3 Operating procedures

The results reported herein are all on steady-state operation. The criterion for effectively attaining the steady

state, which is obvious a priori but has also been demonstrated experimentally [4], is that the operating time t must be long relative to the residence time $\tau = m_b/\dot{m}_p$ of solids in the bed; $t > 2\tau$ is normally sufficient.

Apart from this question of ensuring that collection of the data used fell in the steady state, the operating procedure was straightforward. Product mass fluxes were determined by product collection and periodic weighing. Details of the pilot plant operation have been reported elsewhere [4].

2.4 Particle characterization

Particle size distributions were determined by sieve analysis. The particles were not only of mixed size but also of mixed density and composition:

- from the limestone came calcined and partly sulphated particles of limestone
- from the coal came ash (some fine, some consisting of roasted shale) and char (0.5--3 % of the bed product from the pilot plant runs, and up to 27 % of the cyclone product).

Some of these particles, notably the larger char particles, were relatively fragile. Care was therefore taken in the sieve analysis to minimise further size reduction. The analyses were staged, starting with the coarsest sieves, and the shaking period

was kept suitably short. In some cases the coarsest sieves were shaken by hand to reduce the level of agitation.

Mean particle densities were determined by treating weighed samples consisting of several hundred particles with paraffin or oil to fill the pores and then measuring the total volume by water or methanol displacement. Then $\rho_p = m/V$, where m is the total mass of the particles in the sample and V is the total volume.

3. RESULTS

3.1 Operating conditions and basic characteristics of solid streams

Tables 1 and 2 show the operating conditions of the cold modelling runs and of the pilot plant runs. They also give basic data on the leaving solids streams, namely the mass flux $\dot{m}$ and a characteristic particle diameter $\hat{D}_p$ (defined later herein).

The characterization of recycle level in the pilot plant runs needs explanation. The elutriated dust was partly separated from the exhaust gases by the cyclone, Fig. 1, and virtually all of the rest was separated out by the baghouse. The cycloned dust was partly recycled and partly drawn off as product. In terms of the mass fluxes, then,

$$\dot{m}_e = \dot{m}_c + \dot{m}_r + \dot{m}_h \ , \qquad (2)$$

where $\dot{m}_c + \dot{m}_r$ is the dust flux separated by the cyclone. An index of recycle intensity is the recycle fraction

$$r = \dot{m}_r / (\dot{m}_c + \dot{m}_r) , \qquad (3)$$

i.e., the fraction of the cycloned dust that is recycled. Table 2 shows recycle fractions of 0--0.919. The high level is indeed quite high; it repesents return of over 11 kg dust for every kilogram taken out as cyclone product. Such recycle naturally increases substantially the inventory of dust in the bed.

The last column in Table 2 shows the total mass flux of solid products leaving the pilot plant system,

$$\dot{m}_p = \dot{m}_b + \dot{m}_c + \dot{m}_h . \qquad (4)$$

For the cold model, of course, the feed solids flux $\dot{m}_f$ equalled the product solids flux $\dot{m}_p$. The two systems were operated at roughly comparable solids throughput per unit of bed area; in the pilot plant runs $\dot{m}_p$ = 96--269 kg/hr m^2 and in the cold-model runs $\dot{m}_p$ = 197--1848 kg/hr m^2. The elutriation rates per unit area were respectively 59--388 kg/m^2 and 9.3--1688 kg/m^2.

3.2 Particle characteristics

3.2.1 Measured particle size distributions

Figure 3 shows a typical set of particle size distributions

found in the cold-modelling studies. Comparison of feed and total product indicates significant size reduction (or fines production) occurring in the fluidized bed.

Figures 3 and 4 show similar data for one of the pilot plant runs. Here, of course, the comparison of feed and product is not straightforward and none is shown (we are, though, working on this problem). The size distribution of the elutriated particles, Fig. 5, differs little from that of the cycloned dust, because the baghouse flux was only a small portion (6.4 %) of the whole.

3.2.2 Characteristic particle diameter

A convenient characteristic particle diameter $\hat{D}_p$ is defined by

$$\hat{D}_p = D_p \mid F_D = 1/2 \qquad (5)$$

Values are given for the various streams in Tables 1 and 2. Use of any single characteristic diameter such as this can be quite misleading, of course, when size distributions are dissimilar (not brought nearly into superposition by the normalization $F_D = F_D(D_p/\hat{D}_p)$. However, our results indicate that comparison of values of $\hat{D}_p$ is reasonably meaningful for any single class of FBC solids, such as the elutriated particles.

It was found that there is usually no significant difference

between the size distribution in the bed product (material here extracted by gravity overflow) and material sampled from any point in the bed. Exceptions occurred in the pilot plant runs when very large coal particles ($\hat{D}_p$ = 19.3 mm) were fed. There was then a tendancy for stratification with a growing stagnant layer of correspondingly large shale particles (introduced with the coal) at the bottom of the bed. However, this did not significantly affect conditions higher up.

The solids feed material in the cold-modelling runs, Table 1, was the same in all runs except the last two, the first batch having been exhausted by then. The second batch was not radically different from the first in size distribution. Thus some rough analysis seems permissible in which the feed material is treated as a constant. In this vein, Fig. 6 shows the diameter $\hat{D}_p$ of the elutriated particles as a function of the fluidizing velocity. A relationship

$$\hat{D}_p = 57\ v^{3/2} \qquad (6)$$

is roughly indicated, where D_p and v are respectively in mm and m/s.

3.2.3 Other particle properties

The measurements of mean particle density indicated a value of about 1750 kg/m³ for the cold-modelling feed material, D_p > 1 mm. No significant dependence on particle diameter was found.

Reliable measurements could not be made for particles much smaller than 1 mm dia.

An estimate was also made, based on visual observation and measurements with a travelling microscope, of an average value of the sphericity ϕ, the particle shape factor defined as (surface area of sphere with same volume)/(actual particle surface area). The value found was $\phi = 0.71$.

3.3 Integral leaving flux division

Write $\phi_{st} = \dot{m}_s/\dot{m}_t$ for the ratio of the mass fluxes of the s'th and t'th streams in a process, where t denotes a single reference stream or a combination of streams. Of particular interest here are the following:

- the combustor or column leaving flux fraction

$$\phi^* = \dot{m}_e/(\dot{m}_e + \dot{m}_b) = \dot{m}_e/\dot{m}_l = \phi_{el} \qquad (7)$$

  which measures the division of mass flow between the two leaving solids streams (the elutriated particles and the bed product).

- the system or "plant" leaving flux fraction

$$\phi^* = (\dot{m}_e - \dot{m}_f)/(\dot{m}_b + \dot{m}_e - \dot{m}_f)$$

$$= (\dot{m}_c + \dot{m}_h)/(\dot{m}_b + \dot{m}_c + \dot{m}_h)$$

$$= \dot{m}_o/\dot{m}_p = \phi_{op} \qquad (8)$$

which measures the division of mass flow between the overhead products (cyclone plus baghouse) and the bed product.

The symbols ϕ' and ϕ^* are introduced here just to simplify the notation for these important cases. In the absence of recycle, $\phi' = \phi^*$.

Figure 7 shows that in the cold modelling studies ϕ' (no recycle, so $\phi^* = \phi'$) was only very weakly dependent on bed height, if indeed at all. Figure 8 shows ϕ' for the bed overflow height H_o = 340 mm as a function of the fluidising velocity. At $\phi' < 1/2$, the data are fitted by

$$\phi' = 8.841\ v^{2.4}\ , \qquad (9)$$

v in m/s. The trend at $\phi' > 1/2$ is better judgeable in a representation on logarithmic-probability coordinates, Fig. 9.

Figures 8 and 9 also show ϕ' and ϕ^* for the pilot plant runs. The two results for zero recycle fall very near the curve fitting the cold-modelling data. The results on ϕ^* generally fall much nearer that curve than those on ϕ' and show markedly less scatter. It is interesting that despite the large

differences between the cold-model operating conditions and those of the pilot plant, and despite the fairly broad range in the operating conditions of the pilot plant itself, there are indications of a fairly strong correlation between ϕ^* and v.

3.4 Particle-size resolved leaving flux division

3.4.1 Size resolved fluxes and flux ratios

Write

$$\int_0^\infty \dot{m}_{D,s}\, dD_p = \dot{m}_s \ , \tag{10}$$

where $\dot{m}_{D,s}\, dD_p$ is the mass flux of particles in the diameter range $(D_p,\ D_p + dD_p)$ carried by the s'th solids stream. The relation with the particle size distribution in that stream is

$$\dot{m}_{D,s} = \dot{m}_s \frac{\partial F_{D,s}}{\partial D_p} \tag{11}$$

The size-resolved combustor or column leaving flux fraction of elutriated particles is

$$\phi_D^* = \dot{m}_{D,e}/(\dot{m}_{D,e} + \dot{m}_{D,b}) \ , \tag{12}$$

The analogous system or "plant" flux fraction of overhead products is

$$\phi_D^* = (\dot{m}_{D,e} - \dot{m}_{D,r})/(\dot{m}_{D,b} + \dot{m}_{D,e} - \dot{m}_{D,r})$$

$$= (\dot{m}_{D,c} + \dot{m}_{D,h})/(\dot{m}_{D,b} + \dot{m}_{D,c} + \dot{m}_{D,h})$$

$$= \dot{m}_{D,c}/\dot{m}_{D,p} \qquad (13)$$

In the general resolution of system product fluxes, we may write for the flux fraction of the s'th product stream

$$\phi_{D,sp} = \dot{m}_{D,s}/\dot{m}_{D,p} \qquad (14)$$

In applying the above relations, numerical treatment of our data was of course required. For example, the simplest working form of (11) is

$$\dot{m}_{D,s} = \dot{m}_s \, \Delta F_{D,s}/\Delta D_p \, . \qquad (15)$$

3.4.2 Example of size-resolved product flux division in the pilot plant runs

Figure 10 illustrates the division of size-resolved mass flux between the product streams in the pilot plant runs. The baghouse product is seen to account for a minor fraction of the flux even at small particle diameters, but this is not always the case. In particular, when the cycloned dust is all recycled (r = 1), then the baghouse flux is major at small diameters.

3.4.3 Size-resolved elutriation fluxes in the cold modelling runs

Figure 11 demonstrates that the effect of bed height on the size-resolved elutriation flux fraction, ϕ_D°, was at some particle diameters perceptibly different from that on the integral flux fraction ϕ°, Fig. 7, but still fairly weak. Also shown in the figure are the results for the two pilot plant runs with zero recycle; these seem to fit closely into the pattern of the cold-modelling data.

Figure 12 shows ϕ_D° as a function of the fluidizing velocity v for various particle diameters, at the bed overflow height H_o = 348 mm. From this graph, values of v at ϕ_D° = 1/2 were taken and are shown as a function of the particle diameter D_p in Fig. 13. The data are fitted by

$$v = 8.8149\ D_p^{0.86} . \qquad (16)$$

The correlation is strikingly good. This suggests a transformation of Fig. 12 into the form $\phi_D^\circ = \phi_D^\circ\ (v/D_p^{0.86})$ or better, in order to directly show the relation with particle diameter, $\phi_D^\circ = \phi_D^\circ\ (D_p/v^{1.163})$. The results, Fig. 14, indicate that the correlation holds over the whole range of ϕ_D°.

3.4.4 Time-resolved elutriation fluxes in the pilot plant runs

The fine correlation obtained of the cold-modelling data suggests application of the same scheme to the pilot plant data. The result, Figs. 14 and 15, is equally striking. The data for

zero recycle fall very near the cold-modelling data. Recycle at levels of r = 0--0.6 has apparently no significant effect, Fig. 15. However, sufficiently high levels of recycle do produce a shift, and the results for r = 0.88--0.985 cluster on a curve displaced toward higher $D_p/v^{1.163}$ by a multiplier of about 1.30. Oddly though, the data for the highest recycle, r = 0.919, tend back towards those at low recycle.

4. DISCUSSION

Ability to predict the split of particles between the solids streams leaving the combustor--the elutriated particles and the bed product--represents an effective solution of the problem of elutriation. Two subsidiary problems must also be dealt with, though, in order to complete a predictive procedure; these are:

- characterization of the solid feed materials to determine the product particle population they would produce in the absence of comminution and agglomeration in the fluidized bed. In the case of non-reacting solids, as in the cold modelling studies, this problem is trivial. For an operating FBC system, however, it is far from easy. A part of the solution is to fully burn a sample of coal in a fixed bed in order to obtain a sample of ash representing the "as fed" condition. The most difficult part is the estimation and characterization of combustible residues (char).

- characterization of the processes of comminution (by abrasion

and breakage) and agglomeration (by fusion) in the fluidised bed.

We have begun an examination of these vexing problems and will continue it as more evidence is obtained from our future pilot plant studies. Workers in other laboratories are similarly engaged. The focus of the present paper is, however, entirely on the fate of the particles that are in fact produced, and not on their origin. It appears that in this some success has been achieved. The principal findings are:

1. Analysis based on resolution of particle size seems to be fundamentally necessary in order to expose the mathematical structure of the effects. As a simple illustration, compare Figs. 6 and 13.

2. The present results indicate a remarkably strong correlation between the size-resolved leaving stream division, measured by the flux fraction ϕ_D°, and the variable $D_p/v^{1.163}$. This relation appears to provide a good basis for the prediction of elutriation.

3. There are indications of effects of bed height, but these are mild and of minor importance over the present experimental range of the overflow height, H_o = 168--1200 mm. The magnitude of the effect can be gauged from Fig. 11. The results indicate a maximum in the curve of ϕ_D° vs H_o at constant D_p and v. At

D_p = 350 μm, Fig. 11, this maximum is located at approximately $H_o/v = 0.15\ s^{-1}$.

4. The results for cold model and pilot plant at zero recycle are very close, Fig. 14. This indicates that the features which are different in the pilot-plant operation are of minor or negligible importance: the high temperature of 800--900 °C, the chemical reaction, the 0.5-times greater bed area, the in-bed heat exchange tubes, the multiple point-source type distributor. It is apparent that there should be substantial differences in the quality of fluidization (bubble size, frequency, velocity, growth, and breakup, if one may here think in terms of bubbling fluidization for illustration even though the model may have only small validity for the present operating conditions). It appears, contrary to the expectations of theories attaching importance to bubble eruption in elutriation, that quality of fluidization, too, has small effect so long as a bed is fairly vigorously agitated.

5. Recycle has no apparent effect at recycle fractions r up to 0.6. However, strong recycle (r > 0.8), not unexpectedly, does produce significant change. It increases the amount elutriated, particularly at the larger particle diameters.

It has been observed before [19] that bed diameter negligibly affects elutriation. This in itself is an indication that quality of fluidization is of low importance for

elutriation. The onset of slugging, for example, is evidently quite sensitive to both bed diameter and bed height in the present range of operation. According to Broadhurst and Becker [5], the minimum slugging velocity v_{ms} at $H_s/D_c < 3$ is given by

$$v_{ms} = 5.1\ (D_c/H_s)^{0.895}\ (gD_p)^{1/2}\ , \qquad (17)$$

where D_c is the bed (column or combustor) diameter, and H_s is the settled bed height (established by fluidizing and then slowly reducing the gas flow until the bed comes to rest). For the present conditions, the relation between H_s and the overflow height was roughly $H_s = 0.5\ H_o$, so $H_s/D_c = 0.5$--1.8 in the cold-modelling runs and $H_s/D = 1.4$ in the pilot plant runs.

A further indicator of quality of fluidization is given by the ratio v/v_{mf}, or by $(v - v_{mf})/v_{mf}$. The minimum fluidizing velocities v_{mf} in the cold-modelling runs were 0.23 m/s with the $\hat{D}_p$ = 598 μm feed material, and 0.125 m/s with the 420 μm material. In the pilot plant runs, it was found [4] that v_{mf} = 0.23 m/s when using the $\hat{D}_p$ = 788 μm limestone, and 0.96 m/s for the 1.988 μm stone. Comparing with Tables 1 and 2, it is seen that v/v_{mf} = 4.5--37 in the cold modelling runs and 1.76--12 in the pilot plant runs. The results on elutriation clearly show a strong effect of the fluidizing velocity v, but no apparent effect of v/v_{mf}.

If the correlation in Figs. 14 and 15 is indeed of basic significance, then it should be representable in non-dimensional form. Introducing nothing further beyond the obvious material properties and the gravitational force, we find the attractive possibility

$$\eta = \left(\frac{gD_p}{v^2}\right)^{0.442} \left(\frac{gD_p^3 (\rho_p - \rho_g)}{\mu v}\right)^{0.279}$$

$$= D_p \left(\frac{g}{v^2}\right)^{0.442} \left(\frac{g (\rho_p - \rho_g)}{\mu v}\right)^{0.279}$$

The only temperature-dependent factor in this is the viscosity μ. Assuming that the gases all behave like air, $\mu \propto T^{0.62}$. The factor of $\mu^{-0.279}$ in η thus represents a temperature factor of $T^{-0.173}$. This is consistent with the apparently small or negligible temperature effect in Figs. 14 and 15; a temperature change from 20 °C to 850 °C would appear to produce only a 26 % shift in $d_p/v^{1.63}$ at constant ϕ_D^*.

A generalized correlation of the form $\phi_\eta^* = \phi_\eta^*(\eta)$ is thus suggested. This needs further examination, and a proper understanding of the physical implications may help in constructing a consistent mechanistic model.

ACKNOWLEDGEMENTS

The work on cold modelling was supported by a Strategic Energy Grant from the Natural Sciences and Engineering Research

Council of Canada. The pilot plant combustion trials were carried out under a contract from Supply and Services Canada: DSS Contract Serial No. OSU81-00226, Apr. 1, 1981--Mar. 31, 1983, requisitioned by Energy, Mines and Resources Canada and entitled "Commissioning of a pilot scale fluidized bed combustion research apparatus and conducting of a series of tests to establish a standard test procedure to assess the performance of Canadian limestone and coals in fluid bed combustion". We are grateful to the Scientific Authority assigned to the contract, Dr. E.J. Anthony, for his many contributions to the progress of the research. Mr. David Liang, project engineer on the AFBC pilot plant trials, gave very valuable assistance in the construction of the cold modelling rig.

NOTATION

Subscripts identifying solids streams:

b bed product (solids drawn from the bed, out of the system)

c cyclone product (cycloned dust taken out of the system)

e elutriated solids (leaving the column or combustor, above the transport disengagement height)

f feed material

h beghouse product

i sum of streams leaving the combustor or column (b and e)

o sum of overhead products (c and h)

p sum of products (b, c and h)

r recycle (cycloned dust returned to the bed)

s the s'th solids stream (any of b, c, e, ...)

t the t'th solids stream (may be one of, or any combination of, b, c, e, ...)

Variables (note that while the SI units are shown below, mass fluxes are reported in kg/hr in the text):

A_b bed cross-sectional area, m^2

s,t the s'th and t'th streams in a process (any of b, c, e, ...)

.

Variables:

A_b bed cross-sectional area, m^2

D_c column or combustor chamber diameter. Calculated as

$D_c = (4A_b/\pi)^{1/2}$ for the combustor

D_p particle diameter as determined by sieve analysis, m

$\hat{D}_p$ characteristic particle diameter for a population of particles, m; defined as the value of D_p at $F_D = 1/2$

E_D elutriation coefficient for particles of diameter D_p, $kg/m^2 s$

g acceleration due to gravity, m/s^2

F_D distribution function, $F_D = F_D(D_p)$, of particle size in a population: the mass fraction of particles of size smaller than the argument value of D_p; the "mass fraction undersize". Determined by sieve analysis.

H_o the overflow bed height, m: the vertical distance from the distributor plate to the bottom edge of the bed overflow port

H_s settled bed height, m: the bed height observed after gradually reducing the gas flow until fluidization ceases and the bed comes to rest (becomes "fixed")

m mass, kg

m_b bed mass, kg. The mass "holdup" in the column or combustor

$\dot{m}_s$ mass flux of the s'th solids stream, kg/s. See list of subscripts (above) for labels used for specific streams

$\dot{m}_{D,s}$ diameter-resolved mass flux of the s'th solids stream, kg/m·s: the density function such that $\dot{m}_{D,s}\, dD_p$ is the mass flux of particles in the size range $(D_p,\ D_p + dD_p)$

$(\Delta P)_b$ pressure drop across the bed, Pa

r recycle fraction: the mass fraction of cycloned dust that is returned to the column or combustor

S surface area, m^2

t time, s

v fluidizing velocity, m/s: the superficial gas velocity up the column or combustor defined at bed temperature, bed exit gas composition, and freeboard pressure

v_{mf} minimum fluidizing velocity, m/s: the value of v at the point of incipient fluidization as indicated by the graph of $(-\Delta P)_b$ vs v, following the standard procedure

v_{ms} minimum slugging velocity, m/s: the value of v at the onset of slugging

V volume, m^3

w_D density function, $w_D = w_D(D_p)$, of the particle size in a population, such that $w_D\, dD_p$ is the mass fraction of particles in the diameter range $(D_p,\ D_p + dD_p)$. Determined by sieve analysis, related to the distribution function F_D by $F_D = \int_0^{\infty} w_D\, dD_p$

η $= D_p(g/\nu^2)^{0.442}\ (g(\rho_p - \rho_g)/\rho\nu)^{0.279}$, normalized particle diameter

ϕ_{st} $= \dot{m}_s/\dot{m}_t$, flux ratio of the s'th and t'th solids streams, where t is a single stream or any collection of streams

$\phi_{D,st}$ $= \dot{m}_{D,s}/\dot{m}_{D,t}$, diameter-resolved flux ratio of the s'th and t'th solids streams

ϕ^* $= \phi_{et}$

ϕ^* $= \phi_{op}$

ϕ_D^* $= \phi_{D,et}$

ϕ_D^* $= \phi_{D,op}$

μ gas viscosity, kg/m·s

ν = μ/ρ_g, kinematic gas viscosity, m²/s

ρ_g gas density, kg/m³

ρ_p particle density, kg/m³

τ = $m_b/\dot{m}_p$, mean solids residence time in bed, s

REFERENCES

1. Andrews, M., Ind. Eng. Chem. 52, 85 (1968)

2. Bachovchin, D.M., Beer, J.M., and Sarofim, A.F., AIChE Symposium Series (No. 205) 77, 76 (1981)

3. Becker, H.A. and Code, R.K., The Pilot Plant Installation at Queen's University for Studies of Atmospheric Fluidized Bed Combustion, Tech. Rept. QFBC.TR.82.1, Dept. of Chemical Engineering, Queen's University at Kingston (Kingston, Canada K7L 3N6), 1972

4. Becker, H.A. and Code, R.K., Pilot Scale Trials on Atmospheric Fluidized Bed Combustion of High-Sulphur Eastern Canadian Coals (Minto and Devco) with Limestone Addition for Sulphur Capture, Tech. Rept. QFBC.TR.83.1, Dept. of Chemical Engineering, Queen's University at Kingston (Kingston, Canada K7L 3N6), 1983

5. Broadhurst, T.E. and Becker, H.A., AIChE Jour. 21, 238 (1975)

6. Colakyan, M., Catipovic, N., Javanovic, G. and Fitzgerald, T., AIChE Symposium Series (No. 205) 77, 66 (1981)

7. Geldart, D., Cullinan, J., Georghiades, S., Gilvray, D. and Pope, D.J., Trans.I.Chem.E. 57, 269 (1979)

8. George, S.E. and Grace, J.R., Can.J.Chem.Eng. 59, 279 (1981)

9. Gugnoni, R.J. and Zenz, F.A., Fluidization (Grace, J.R. and

Matsen, J.M., eds.), P. 501, Plenum Press, 1988

10. Morio, M., Taki, A., Hsieh, Y.S. and Muchi, I., Fluidization (Grace, J.R. and Matsen, J.M., eds.), p. 589, Plenum Press, 1988

11. Kunii, D. and Levenspiel, O., J.Chem.Eng.Japan 2, 84 (1969)

12. Lewis, W.K., Gilliland, E.R. and Lang, P.M., Chem. Eng. Prog. Symp. Ser. (No. 38) 58, 65 (1962)

13. Lin, L., Sears, J.T. and Wen, C.Y., Powder Technology 27, 105 (1980)

14. Lowell, C.E. and Wormser, A.F., Proc. 7th International Conference on Fluidized Bed Combustion (DOE/METC/83-48, available from National Technical Information Service, U.S. Dept. of Commerce, 5285 Port Royal Road, Springfield, VA 22191), p. 781, 1982

15. Merrick, D. and Highley, J., AIChE Symp. Ser. (No. 137) 70, 366 (1974)

16. Nazemi, A., Bergougnou, M.A. and Baker, C.G., AIChE Symp. Ser. (No. 141) 70, 98 (1974)

17. Osberg, G.L. and Charlesworth, D.H., Chem. Eng. Prog. 74, 566 (1951)

18. Tanaka, I. and Shinohara, H., J.Chem.Eng.Japan 5, 57 (1972)

19. Wen, C.Y. and Hashinger, E.F., AIChE Jour. 6, 220 (1960)

20. Yagi, S. and Aochi, T., Paper presented to the Society of Chemical Engineers (Japan), Spring Meeting, 1955

21. Zenz, F.A. and Weil, N.A., AIChE Jour. 4, 472 (1958)

Table 1. Operating conditions and characteristics of solids streams in the cold-modelling runs.

		Feed		Bed product		Elutriated	
H_o cm	v m/s	$\dot{m}_f$ kg/hr	$\hat{D}_p$ μm	$\dot{m}_b$ kg/hr	$\hat{D}_p$ μm	$\dot{m}_e$ kg/hr	$\hat{D}_p$ μm
16	1.05	3.6	590	3.4	560	0.18	69
34	1.05	3.6	590	3.4	570	0.17	65
55	1.05	3.8	590	3.6	560	0.18	66
16	1.55	5.7	590	5.0	630	0.65	93
34	1.55	5.7	590	5.1	610	0.61	96
55	1.55	6.0	590	5.4	590	0.61	99
16	2.00	9.2	590	7.0	580	2.23	230
34	2.00	9.1	590	6.8	610	2.27	190
55	2.00	9.4	590	7.2	610	2.23	185
34	2.00	7.5	590	5.2	810	2.26	182
34	2.77	23.3	420	13.2	640	10.1	265
34	4.64	33.5	420	4.3	850	29.2	410

Table 2. Operating conditions and characteristics of solids streams in the pilot plant combustion runs.

	Coal		Stone						Bed product		Elutriated		Recycle	Prod.
Run	$\hat{D}_p$ mm	$\dot{m}$ kg/hr	$\hat{D}_p$ μm	$\dot{m}$ kg/hr	Ca/S	r	T_b °C	v m/s	$\dot{m}_b$ kg/hr	$\hat{D}_p$ μm	$\dot{m}_e$ kg/hr	$\hat{D}_p$ μm	$\dot{m}_r$ kg/hr	$\dot{m}_p$ kg/hr
830106	18.7	27.9	1900	12.5	2.06	0.80	845	1.69	12.0	870	18.9	95	8.1	14.9
830124	18.7	32.8	700	15.0	2.18	0.905	820	1.86	12.4	630	42.4	55	37.2	17.6
830126	18.7	38.3	700	20.0	4.25	0.836	805	1.75	16.6	570	44.5	59	35.2	27.3
830127	18.7	38.3	700	18.5	2.66	0.875	835	1.79	13.0	590	34.2	80	28.0	23.7
830201	6.6	33.3	700	17.5	2.24	0.919	825	1.86	12.5	540	46.6	52	40.0	19.1
830215	6.6	41.0	700	21.6	2.24	0.60	860	2.77	13.0	750	25.7	67	13.5	25.2
830216	6.6	40.9	700	20.0	2.92	0.52	865	2.76	15.7	730	29.2	70	13.0	22.3
830217	6.6	39.0	700	27.6	2.95	0	840	2.70	15.1	770	15.0	90	0	38.9
830218	19.3	30.0	1900	23.3	2.70	0	860	2.77	16.2	1160	9.2	90	0	25.4
830224	19.3	38.0	1720	38.7	3.56	0.57	855	2.68	21.0	1250	20.4	60	10.6	40.3

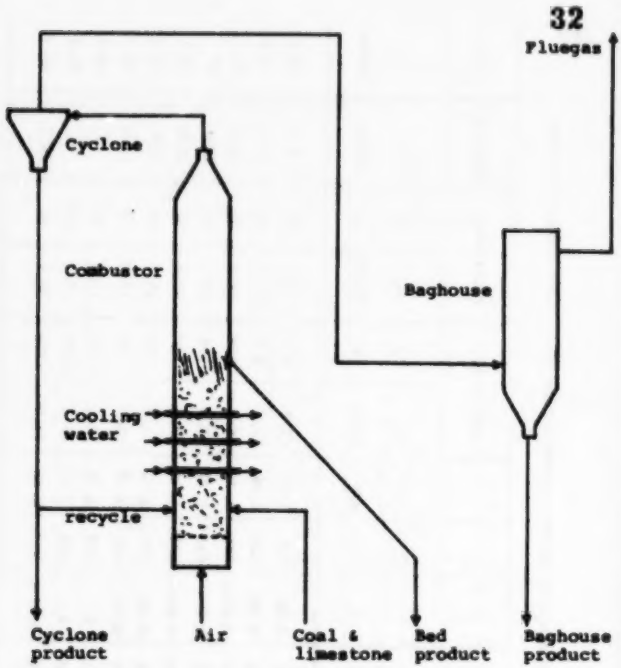

Fig. 1. Schematic representation of the AFBC pilot plant.

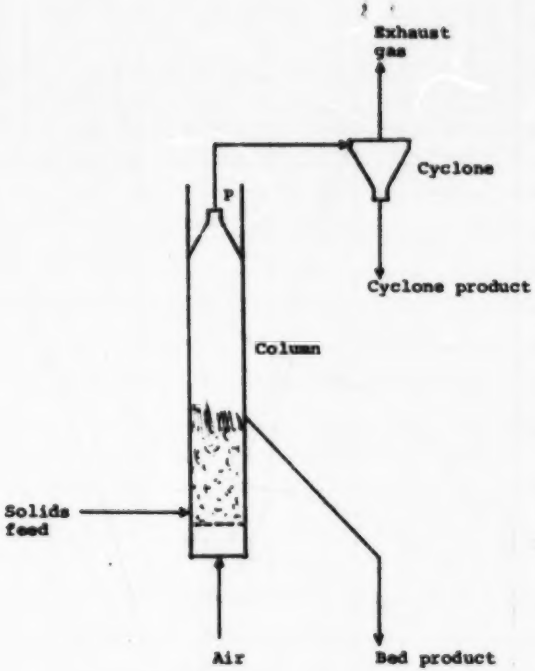

Fig. 2. Schematic representation of the AFBC cold modelling rig. The conical probe P collects the whole freeboard gas flow and passes it on to the cyclone dust separator.

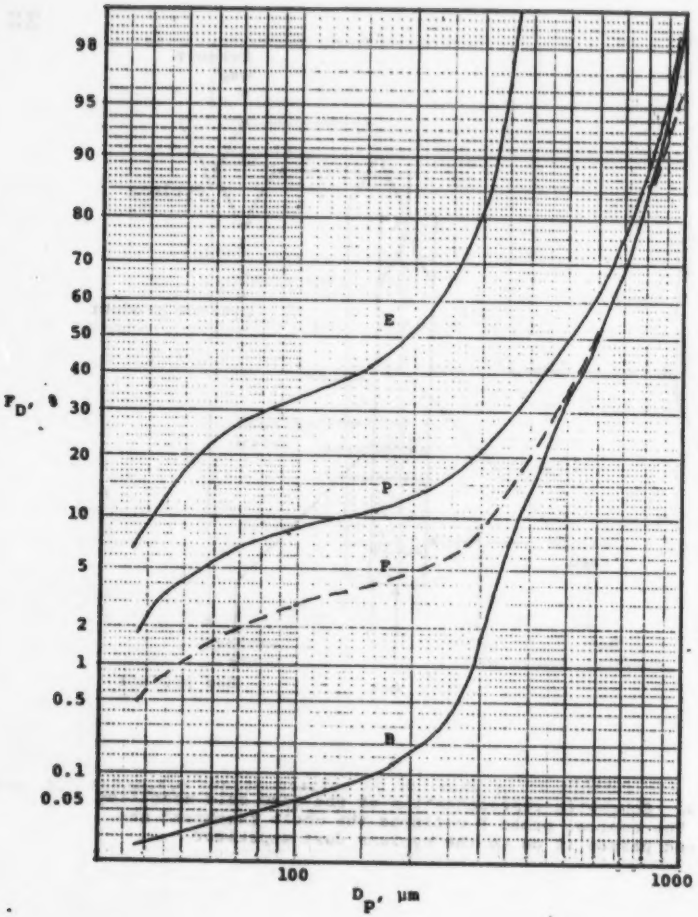

Fig. 3. Example of particle size distributions in the cold-modelling runs (the eighth run in Table 1). Curves: F, feed; E, elutriated solids; B, bed product; P, total product (B and E combined). Grid: logarithmic/probability.

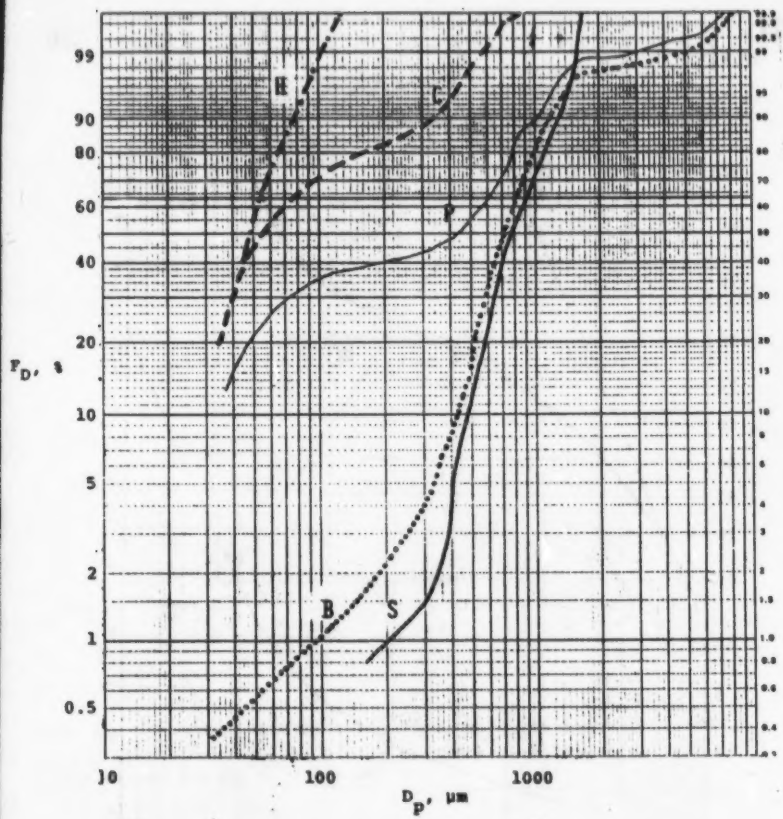

Fig. 4. Example of particle size distributions in the pilot plant combustion trials: Run 830216, Table 2. Curves: S, limestone as fed; B, bed product; C, cyclone product (and recycle); H, baghouse product; P, total product (B, C and H combined). Grid: Rosin-Rammler.

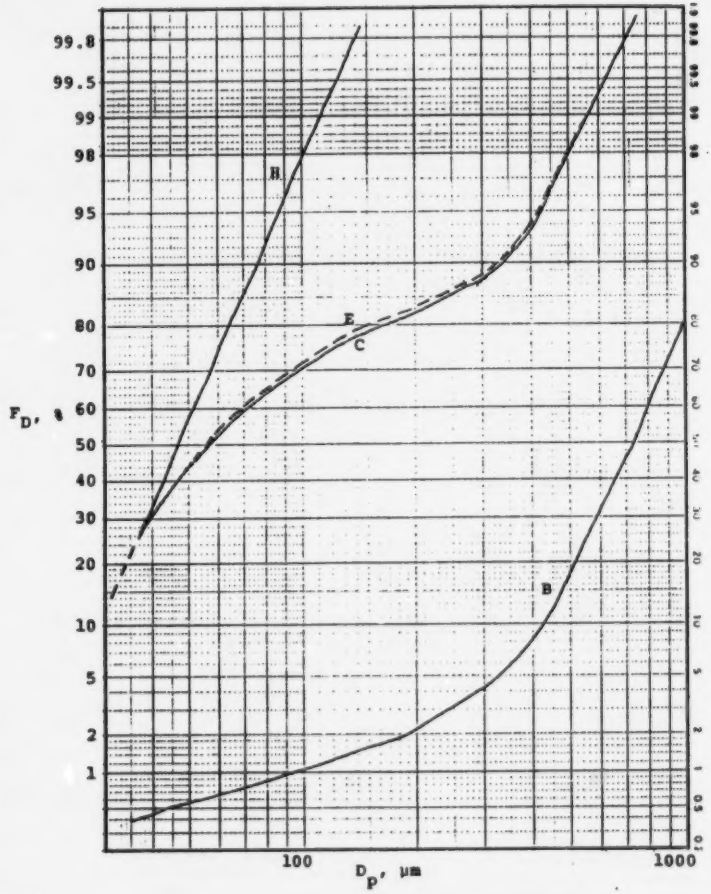

Fig. 5. Example of particle size distribution in the pilot plant trials, Run 830216, Table 2 (same as in Fig. 3). Curves: B, bed product; C, cyclone product; H, baghouse product; E, elutriated solids (C, H, and recycle combined). Grid: logarithmic/probability.

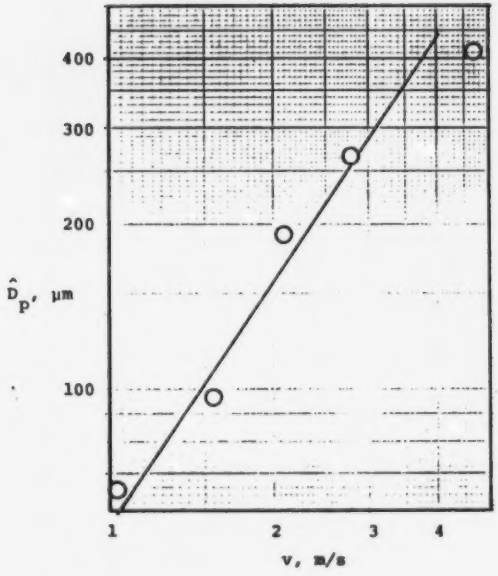

Fig. 6. Characteristic particle diameter $\hat{D}_p$ of the elutriated solids vs fluidizing velocity in the cold-modelling runs, for overflow bed height H_o = 340 mm.

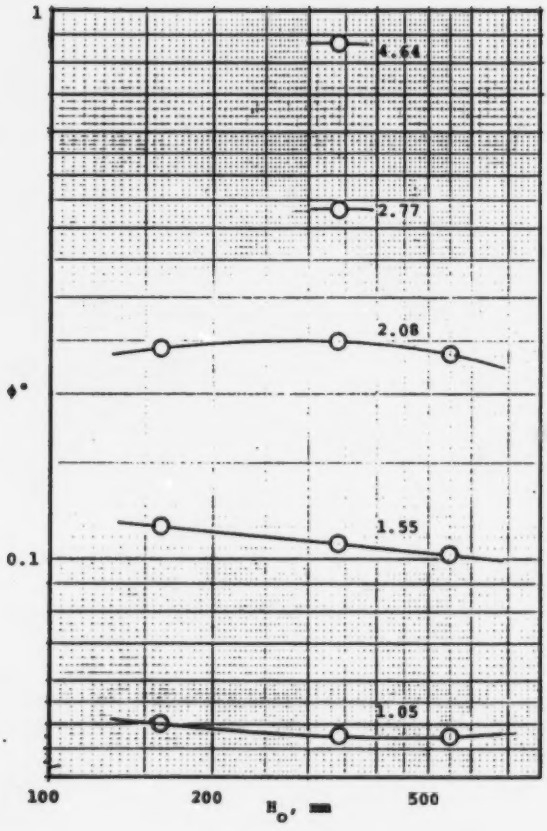

Fig. 7. Effluent mass flux fraction of elutriated particles vs overflow bed height for the cold-modelling runs, with fluidizing velocity v, m/s, as parameter.

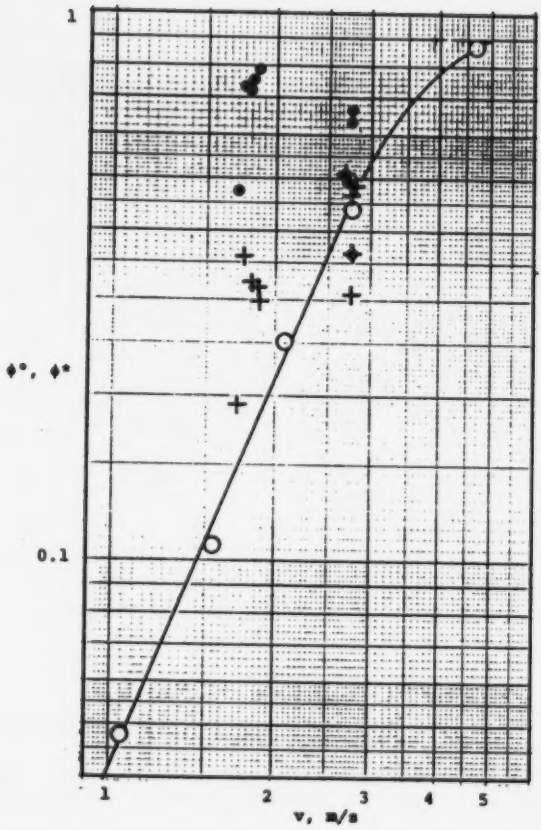

Fig. 8. Leaving stream mass flux fraction vs fluidizing velocity. Data symbols:

○ , ϕ° in the cold-modelling runs at H_o = 348 mm

● , ϕ° in the pilot plant runs

\+ , ϕ^{*} in the pilot plant runs

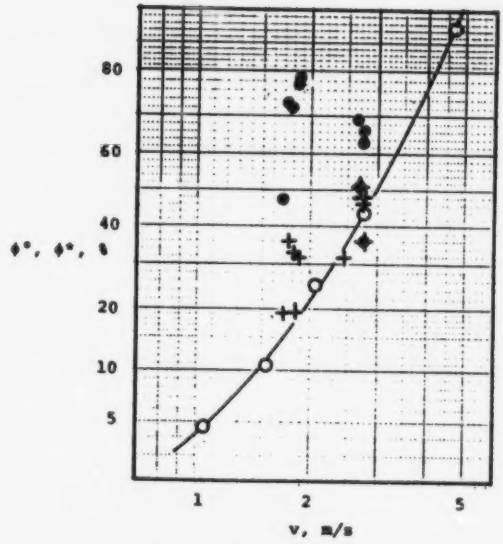

Fig. 9. Same data as in Fig. 8, on logarithmic probability coordinates.

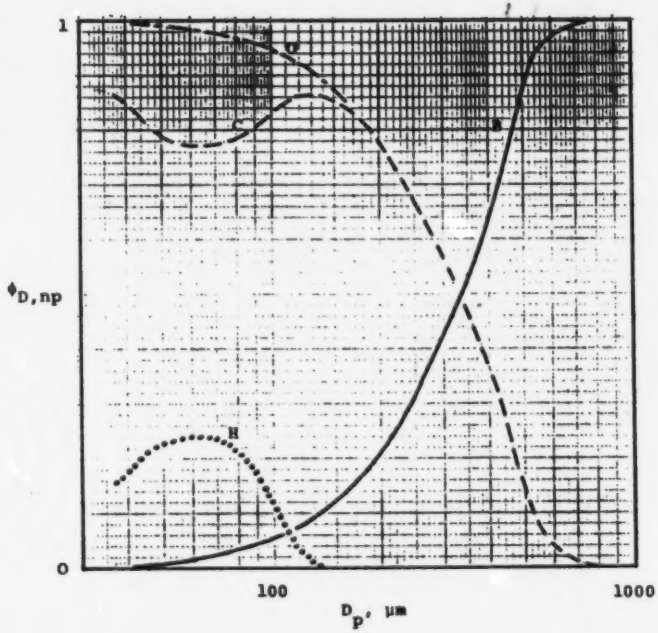

Fig. 18. Example of size-resolved product mass flux division, Run 830216. Curves: B, bed product; C, cyclone product; H, baghouse product; O, overhead products (C and H combined).

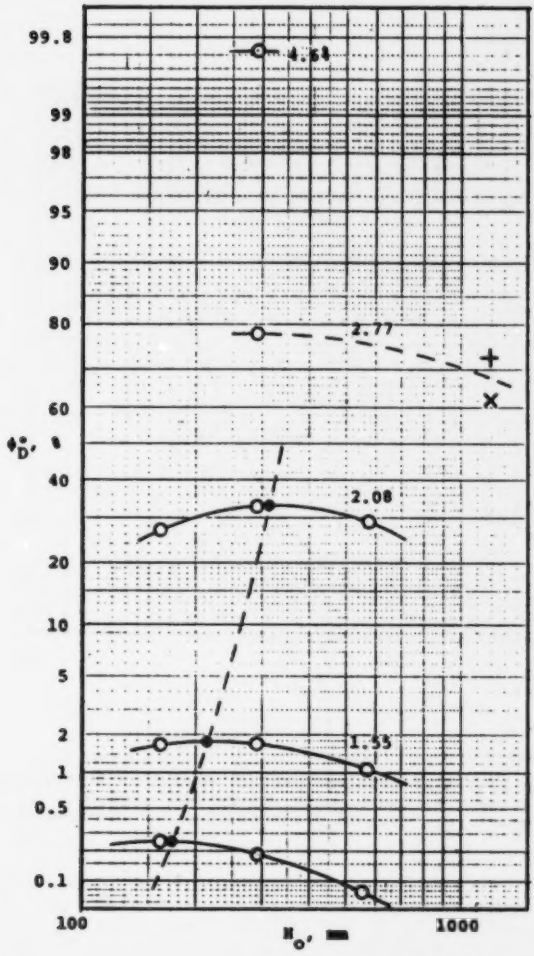

Fig. 11. Size-resolved mass flux fraction of elutriated particles of diameter D_p = 358 μm, as a function of the overflow bed height with the fluidizing velocity v, m/s, as parameter, for the runs without recycle (all the cold modelling runs, symbol O, and two pilot plant runs, symbols +, ×). The filled circles represent maxima. Grid: logarithmic/probability.

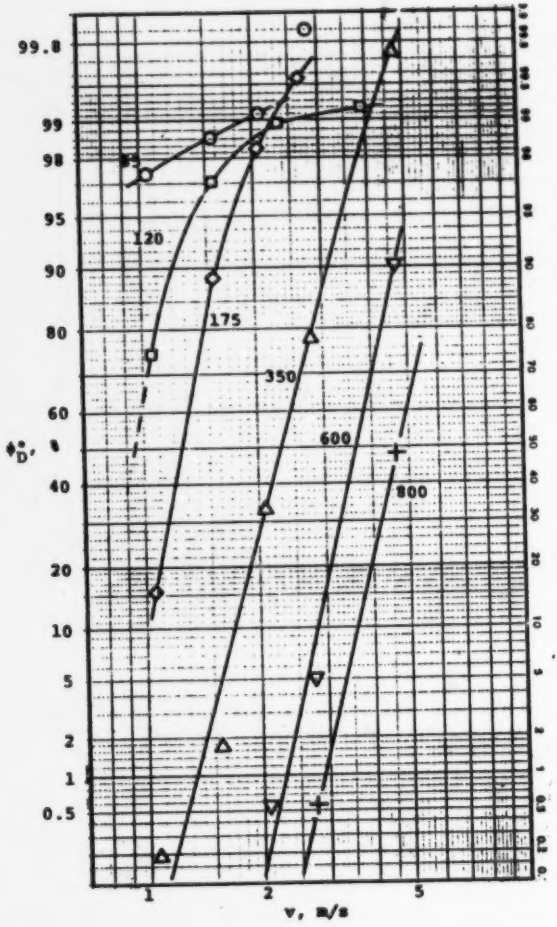

Fig. 12. Size-resolved mass flux fraction of elutriated particles as a function of fluidizing velocity, with particle diameter D_p, μm, as the parameter, at overflow bed height H_o = 348 mm, for the cold-modelling runs. Grid: logarithmic/probability.

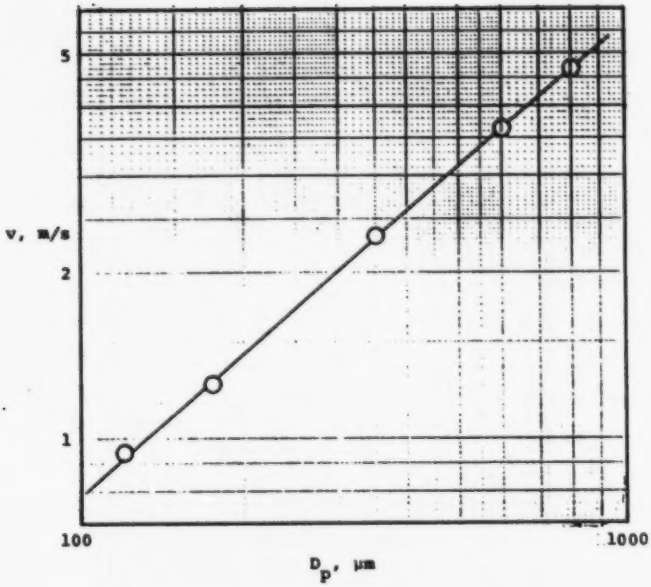

Fig. 13. From Fig. 12, the fluidizing velocity at $\phi' = 1/2$ vs particle diameter, for the cold-modelling runs at overflow bed height H_o = 348 mm.

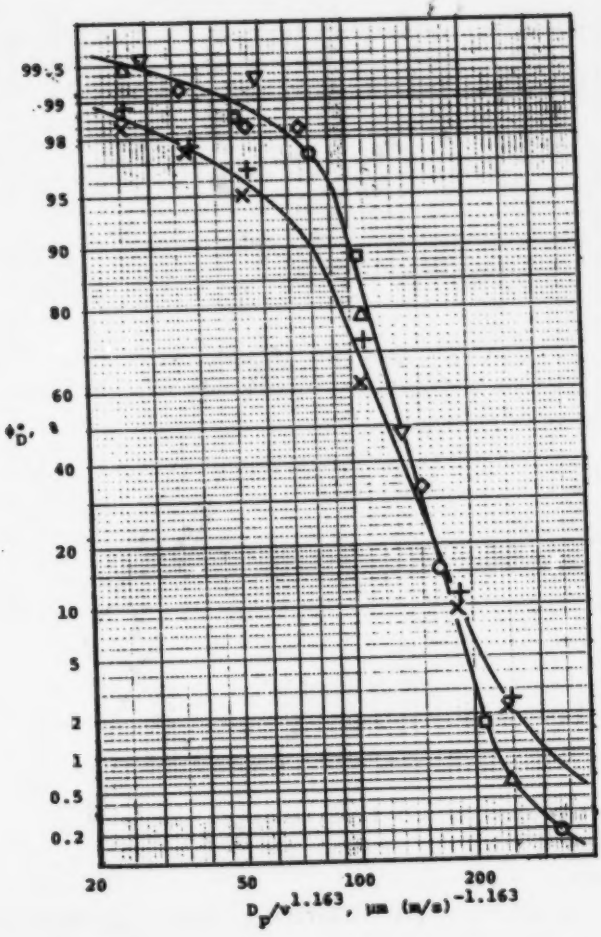

Fig. 14. Size-resolved mass flux fraction of elutriated particles vs $D_p/v^{1.163}$, cold modelling data for H_o = 348 mm and pilot plant data for H_o = 1198 mm, all with zero recycle. Grid: logarithmic/probability.

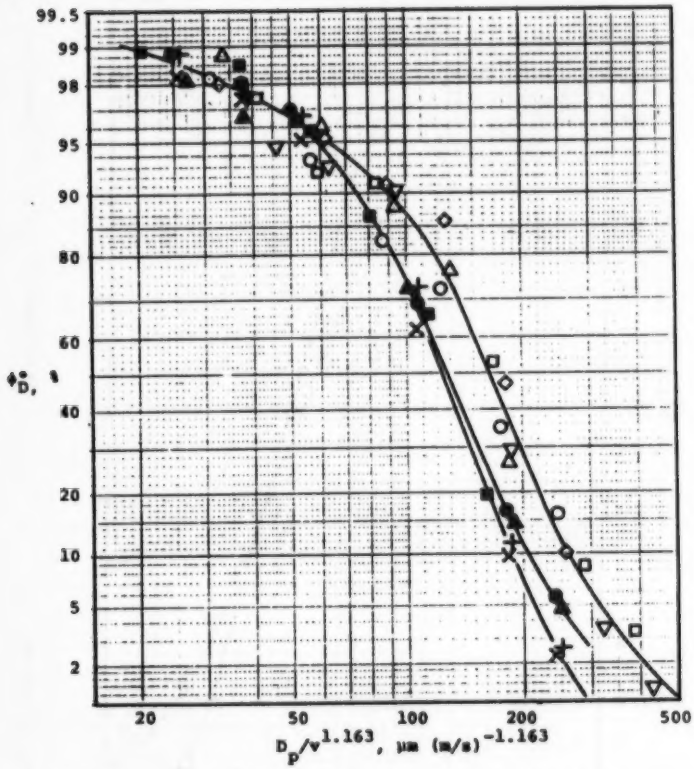

Fig. 15. Size-resolved mass flux fraction of elutriated particles vs $D_p/v^{1.163}$, pilot plant data.

Data symbols:

Run	830201	830124	830127	830126	830106
r	0.919	0.905	0.875	0.836	0.80
Symbol	○	□	◇	△	▽
Run	830215	830224	830216	830217	830218
r	0.68	0.57	0.52	0	0
Symbol	●	■	▲	+	×

POOR

QUALITY

ORIGINAL